Aerial Photographs Reveal Late–20th-Century Dynamic Ice Loss in Northwestern Greenland

Kurt H. Kjær *et al.*

Science **337**, 569 (2012);
DOI: 10.1126/science.1220614

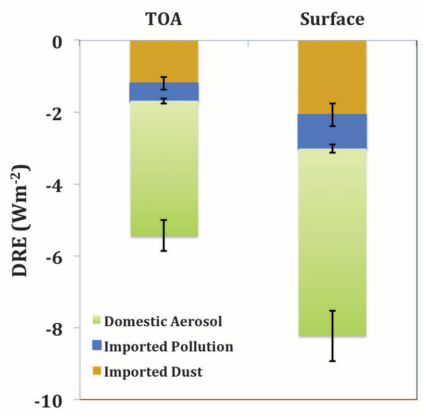

Fig. 4. Estimated clear-sky DRE (watts per square meter) on solar radiation at top-of-atmosphere (TOA) and surface by imported pollution and dust, as well as North American domestic aerosol. Collectively imported dust and pollution aerosols contribute 24 to 41% and 28 to 48% of aerosol-induced total reduction of solar radiation at TOA and surface, respectively. Error bars indicate the range of DRE for perturbing aerosol single-scattering albedo by ±0.03.

America also affect other regions via intercontinental transport. To mitigate aerosol impacts on regional climate change, actions by a single nation are inadequate. The world must work cooperatively and act synchronically to meet the challenges of global health on a changing planet. Focusing on the carbon budget and urban/industrial pollution sources is also inadequate because the imported dust dominates the mass budget and aerosol DREs. Dust emissions can respond to climate changes, such as changes of wind, precipitation, and vegetation. It is thus essential to acquire better understanding of the interactions between dust and climate.

References and Notes

1. J. M. Prospero, E. Blades, G. Mathison, R. Naidu, *Aerobiologia* **21**, 1 (2005).
2. P. E. Biscaye, F. E. Grousset, A. M. Svensson, A. Bory, L. A. Barrie, *Science* **290**, 2258 (2000).
3. R. B. Husar *et al.*, *J. Geophys. Res.* **106**, 18317 (2001).
4. C. L. Heald *et al.*, *J. Geophys. Res.* **111**, D14310 (2006).
5. M. Chin, T. Diehl, P. Ginoux, W. Malm, *Atmos. Chem. Phys.* **7**, 5501 (2007).
6. J. Liu, D. L. Mauzerall, L. W. Horowitz, *Atmos. Chem. Phys.* **8**, 3721 (2008).
7. F. Dentener, T. Keating, H. Akimoto, Eds., *Hemispheric Transport of Air Pollution* (Air Pollution Studies No. 17, United Nations, Geneva, 2010).
8. H. Yu *et al.*, in *Atmospheric Aerosol Properties and Climate Impacts, A Report by the U.S. Climate Change Science Program and the Subcommittee on Global Change Research*, M. Chin, R. A. Kahn, S. E. Schwartz, Eds. (NASA, Washington, DC, 2009).
9. O. V. Kalashnikova, R. A. Kahn, *J. Geophys. Res.* **113**, D24204 (2008).
10. Z. Liu *et al.*, *J. Geophys. Res.* **113**, D07207 (2008).
11. Y. J. Kaufman *et al.*, *J. Geophys. Res.* **110**, D10S12 (2005).
12. H. Yu *et al.*, *J. Geophys. Res.* **113**, D14S12 (2008).
13. L. A. Remer *et al.*, *J. Geophys. Res.* **113**, D14S07 (2008).
14. D. M. Winker *et al.*, *Bull. Am. Meteorol. Soc.* **91**, 1211 (2010).
15. Materials and methods are available as suppplementary materials on *Science* Online.
16. H. Yu *et al.*, *J. Geophys. Res.* **114**, D10206 (2009).
17. C. Warneke *et al.*, *Geophys. Res. Lett.* **36**, L02813 (2009).
18. J. L. Stith *et al.*, *J. Geophys. Res.* **114**, D05207 (2009).
19. A. Zhu, V. Ramanathan, F. Li, D. Kim, *J. Geophys. Res.* **112**, D16208 (2007).
20. L. Su, O. B. Toon, *Atmos. Chem. Phys.* **11**, 3263 (2011).
21. H. Maring, D. L. Savoie, M. A. Izaguirre, L. Custals, J. S. Reid, *J. Geophys. Res.* **108**, 8592 (2003).
22. M. Chin *et al.*, *Ann. Geophys.* **27**, 3439 (2009).
23. H. Bian *et al.*, *Atmos. Chem. Phys.* **9**, 2375 (2009).
24. T. F. Eck *et al.*, *J. Geophys. Res.* **110**, D06202 (2005).
25. V. Ramanathan, G. Carmichael, *Nat. Geosci.* **1**, 221 (2008).
26. H. Yu, S. C. Liu, R. E. Dickinson, *J. Geophys. Res.* **107**, 4142 (2002).
27. K. Sassen, *Geophys. Res. Lett.* **29**, 1465 (2002).
28. O. L. Hadley, C. E. Corrigan, T. W. Kirchstetter, S. Cliff, V. Ramanathan, *Atmos. Chem. Phys.* **10**, 7505 (2010).

Acknowledgments: We acknowledge the NASA support of this work via NNXAH66G (The Science of Terra and Aqua Program) and NNX11AJ91G (Atmospheric Composition Modeling and Analysis Program) (H.Y.), both managed by R. Eckman. The NASA Modeling, Analysis, and Prediction program managed by D. Considine is acknowledged for supporting the model development of GOCART (M.C.) and GMI (H.B., under NNX10AK61G). We are grateful to J. Zhang for providing his reprocessed MODIS data, Z. Liu for providing insights in the lidar characterization of Asian dust, and X. Pan for acquiring CALIOP data. The MODIS data were obtained from the NASA Level 1 and Atmosphere Archive and Distribution System. The CALIOP data were obtained from the NASA Langley Research Center Atmospheric Science Data Center.

Supplementary Materials

www.sciencemag.org/cgi/content/full/337/6094/566/DC1
Materials and Methods
Figs. S1 to S6
References (*29*–*46*)

6 December 2011; accepted 12 June 2012
10.1126/science.1217576

Aerial Photographs Reveal Late–20th-Century Dynamic Ice Loss in Northwestern Greenland

Kurt H. Kjær,[1]* Shfaqat A. Khan,[2] Niels J. Korsgaard,[1] John Wahr,[3] Jonathan L. Bamber,[4] Ruud Hurkmans,[4] Michiel van den Broeke,[5] Lars H. Timm,[1] Kristian K. Kjeldsen,[1] Anders A. Bjørk,[1] Nicolaj K. Larsen,[6] Lars Tyge Jørgensen,[7] Anders Færch-Jensen,[7] Eske Willerslev[1]

Global warming is predicted to have a profound impact on the Greenland Ice Sheet and its contribution to global sea-level rise. Recent mass loss in the northwest of Greenland has been substantial. Using aerial photographs, we produced digital elevation models and extended the time record of recent observed marginal dynamic thinning back to the mid-1980s. We reveal two independent dynamic ice loss events on the northwestern Greenland Ice Sheet margin: from 1985 to 1993 and 2005 to 2010, which were separated by limited mass changes. Our results suggest that the ice mass changes in this sector were primarily caused by short-lived dynamic ice loss events rather than changes in the surface mass balance. This finding challenges predictions about the future response of the Greenland Ice Sheet to increasing global temperatures.

Mass loss from the Greenland Ice Sheet is a complex function of processes related to surface mass balance (SMB) and dynamic ice loss (DIL) that are forced by fluctuations in atmospheric and oceanic energy input (*1*). SMB is the difference between accumulation from solid precipitation (snow) and mass loss from ablation (ice melt and sublimation). DIL is related to marine-terminating outlets due to the marginal breakup of floating ice tongues and to subsequent accelerated flow caused by decreased buttressing and reduced basal drag, resulting in thinning (decreasing ice surface elevations) (*2*–*4*). The relative role of SMB to DIL in contributing to marginal ice mass loss remains contentious (*5*–*7*).

Only limited observational evidence of ice mass changes exists before the 21st century, when space-based observations from interferometric synthetic aperture radar (InSAR), intensity tracking

[1]Centre for GeoGenetics, Natural History Museum, University of Copenhagen, Copenhagen, Denmark. [2]DTU Space–National Space Institute, Technical University of Denmark, Department of Geodesy, Lyngby, Denmark. [3]Department of Physics and Cooperative Institute for Research in Environmental Sciences, University of Colorado, Boulder, CO, USA. [4]Bristol Glaciology Centre, University of Bristol, Bristol, UK. [5]Institute for Marine and Atmospheric Research, Utrecht University, Utrecht, Netherlands. [6]Department of Geoscience, Aarhus University, Aarhus, Denmark. [7]Danish National Cadastre and Survey, Copenhagen, Denmark.

*To whom correspondence should be addressed. E-mail: kurtk@snm.ku.dk

on SAR images, GRACE (Gravity Recovery and Climate Experiment), and ICESat (Ice, Cloud and land Elevation Satellite) became available. Together with data from the Global Positioning System (GPS), these data, when interpreted as a sustained and accelerating induced loss of the Greenland Ice Sheet (*5*, *8*–*10*) (Fig. 1), suggest potentially severe consequences for global sea-level rise (*9*, *11*–*13*). However, the current records

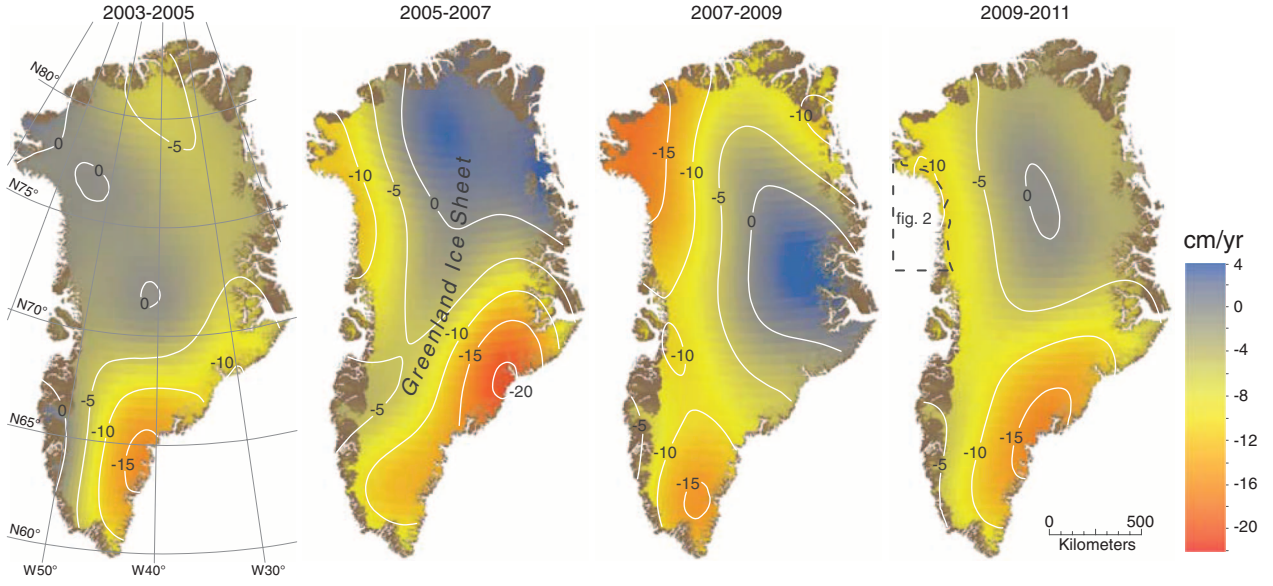

Fig. 1. Catchment-wide mass change of the Greenland Ice Sheet extracted from GRACE for 2003–2011, in units of centimeters per year of water thickness, inferred from consecutive 2-year periods (from April to April). The gravity data are provided in monthly sets of spherical harmonic coefficients. Coefficients are transformed into surface mass coefficients, used for computing surface mass on a 0.5° × 0.5° grid and smoothed with a Gaussian smoothing function with a 250-km half-width (*25*).

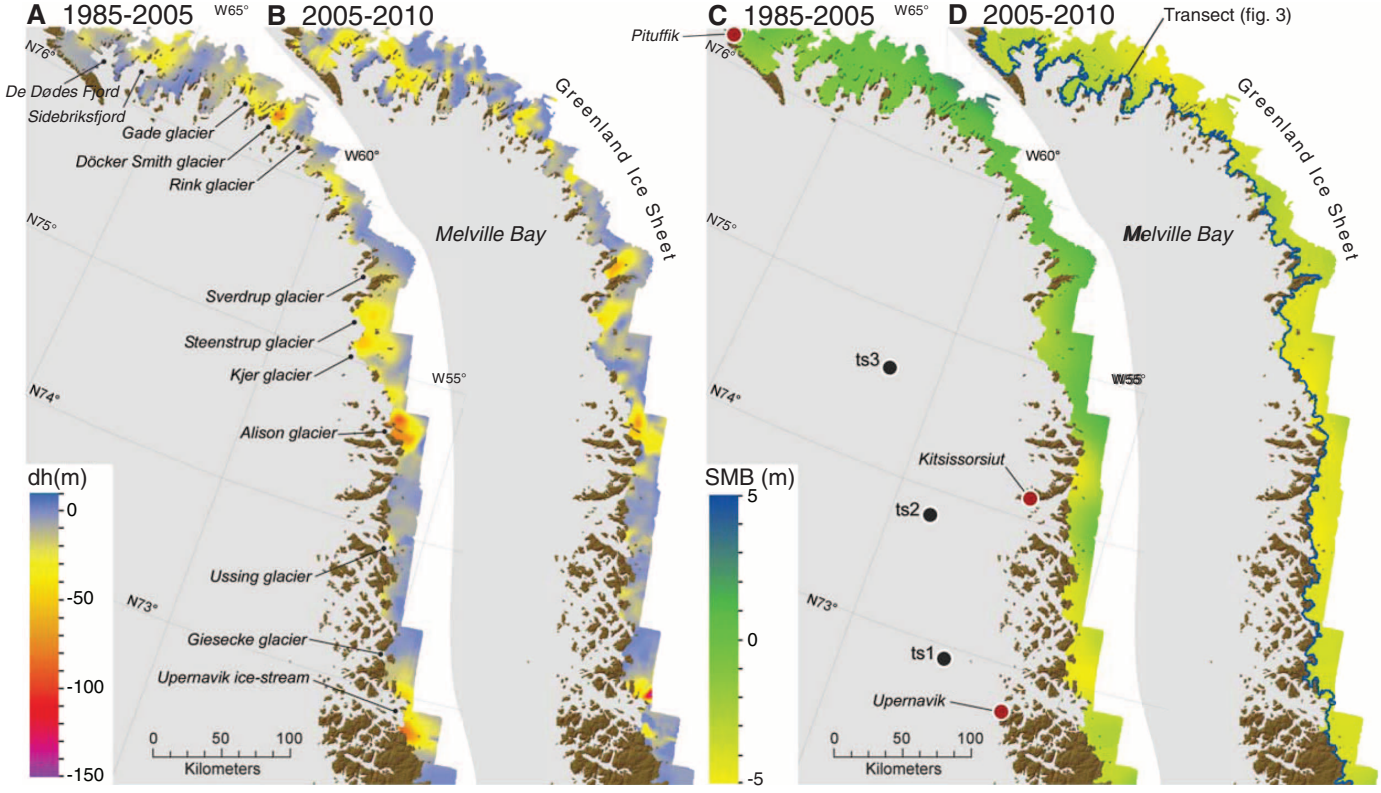

Fig. 2. Total surface elevation changes (dh) derived from DEMs generated from aerial photographs recorded in 1985, ICESat data from 2005, and ATM data from 2005 and 2010. (**A**) dh for the 1985–2005 period. (**B**) dh for the 2005–2010 period. For the same area, the total surface elevation change due to SMB processes was derived from RACMO2, using SMB anomalies from the mean for 1961–1990. (**C**) dh SMB for the 1985–2005 period. (**D**) dh SMB for the 2005–2010 period. Oceanic temperature stations (ts's 1 to 3) are marked on the map, together with air temperature records from meteorological stations in Upernavik, Kitsissorsuit, and Pituffik. Results are displayed in Fig. 4.

suffer from the lack of multidecadal observational data, making any such interpretation tentative (*9*, *12*).We extended the record of DIL back almost threefold (1985–2010) for northwestern Greenland, using a digital elevation model (DEM) derived from aerial photographs.

Figure 2 shows the cumulated elevation difference (dh) during 1985–2005 and 2005–2010 for the northwest margin of the Greenland Ice Sheet. Vertical aerial photographs served as the primary source for the elevation model from 1985 (supplementary materials) (fig. S1). We used these data to derive a 25 × 25–m gridded DEM with elevation referenced to the height above the ellipsoid (WGS84). Digital elevation products from aerial photographs are limited to areas below the snow line, because the low contrast for imagery of snow prevents data sampling. Consequently, the 1985 DEM reaches a maximum of 40 to 50 km inland of the 1985 ice margin frontal position. Comparative DEMs were derived from laser altimetry data recorded in 2005 and 2010: ICESat GLA12 Release 31 data (*14*), complemented by NASAs Airborne Topographic Mapper (ATM) flight lines, which were especially dense in 2010 (*15*) (supplementary materials). The mean vertical accuracy of the 1985 DEM on ice is estimated to 4.1 m, based on validation with the ATM laser altimetry data on ice-free land, with an inherent vertical accuracy of 0.2 m (figs. S2 and S3). We interpolated the observed thinning values to a 25-m grid resolution. Figure S4 shows the predicted uncertainties associated with the interpolated thinning values shown in Fig. 2, A to D. We find pronounced thinning along the entire northwest ice sheet margin over the past 25 years, ranging from tens of meters over nonchannelized areas to 100 to 150 m at a majority of outlet glaciers (Fig. 2, A and B).Thinning is apparent in both the 1985–2005 and 2005–2010 periods, although the detailed thinning pattern is somewhat different across the different glacier outlet systems (figs. S5 to S7).

Figure 3 shows a transect mirroring the ice margin from north to south, where the ice elevation changes (dh) are shown above the *x* axis, and the corresponding ice margin retreat (dl) is shown below the axis, for every 500 m along the transect. Three interesting observations are revealed. First, different tributaries within a single ice stream system can exhibit different rates of thinning and calving-front retreat. For the Upernavik ice stream, for example, the southern tributary shows considerable thinning and frontal retreat between 1985 and 2005 (fig. S5), whereas the other three tributaries experience only limited elevation change. Subsequently, in 2005–2010, the northern tributary shows a pronounced 5500 m of retreat and vertical lowering of ~150 m. The most recent event also coincides with the speed-up of several glaciers along the northwest coast of Greenland (*10*). Second, for most glaciers, pre-2005 thinning and margin retreat were succeeded by further mass loss and retreat after 2005. This is particularly evident for the Alison glacier and its northern neighboring glacier, which show maximum thinning of ~90 and 150 m, respectively, for 1985–2005 and 1985–2010 (Figs. 2 and 3 and fig. S6). Third, the lowering of glacier surfaces was commonly stronger during the second event. The Sverdrup glacier north of Kjer and Steenstrup glaciers retreated 2500 m in the period 1985–2005,

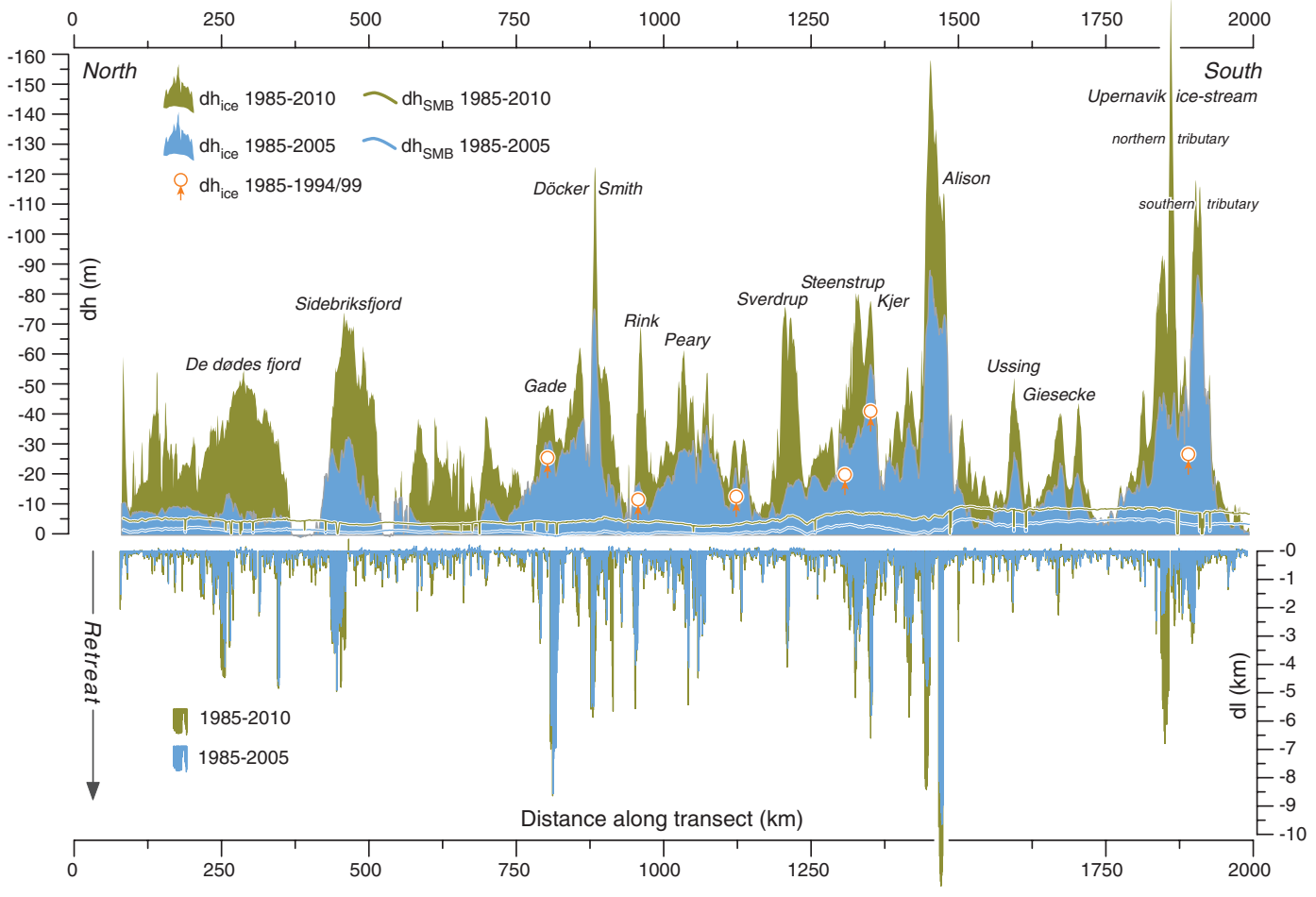

Fig. 3. North-to-south–striking ice marginal transect along the northwest Greenland Ice Sheet superimposed on elevation difference (dh in meters) values from 1985–2005 and 1985–2010, as well as glacier length changes (dl in kilometers) for the same ice frontal sections. The transect is a smoothed line 200 m inland from the 2010 ice margin. The transect provides a spatial resolution of 500 m along the ~2000-km ice sheet margin, providing roughly 4000 frontal positions. Each frontal position is measured perpendicular to the ice sheet margin from a static point placed on the transect.

while the surface lowering amounted to merely 10 m (fig. S7, area 3). The front continued to retreat an additional 1000 m between 2005 and 2010, while the decrease in surface elevation accelerated, with an additional 80 m of lowering.

In order to separate DIL from SMB, we used SMB values for the exact same coverage and periods as the 1985 DEMs, from the Regional Atmospheric Climate Model v.2 (RACMO2), which is based on the High Resolution Limited Area Model (HIRLAM), with physical processes adopted from the global model of the European Centre for Medium-Range Weather Forecasts and modified to reflect surface conditions on the Greenland Ice Sheet (*16*–*18*) (fig. S4). Figure 3 displays the cumulative SMB anomalies along the ice marginal transect, translated to elevation differences with the use of a modeled firn density based on an empirical relationship with firn temperature (*19*, *20*) to enable a direct comparison between surface changes. The former are in general much smaller than the total observed elevation change and have been subtracted from the DEM results. All dh values above a few tens of meters are correlated with fast-flowing areas of the ice margin (*10*), which in turn match areas of conspicuous glacier retreat. The implication is that the significant thinning of the northwest ice margin was mainly driven by DIL, which is supported by recent ICESat estimates (*5*) and velocity mapping (*10*).

Using GRACE for the northwest drainage basin, we find an annual mass loss rate of –46.4 ± 8.9 Gt year^{-1} within the most recent period 2005–2010, which is comparable to previous estimates obtained from the northwest drainage basin using GRACE and ICESat (Table 1). The DEM results show the importance of the marginal area in mass balance estimates: 77% of the total mass reduction is accounted for by the marginal zone relative to the whole drainage basin, which amounts to 35.8 ± 10.3 Gt year^{-1} (the total mass loss from the colored region shown in Fig. 2), relative to 46.4 ± 8.9 Gt year^{-1} (the GRACE estimate of the total northwest mass loss).

We observe rapid dynamic induced ice loss during 2005–2010 of 25.5 ± 10.4 Gt year^{-1} (the total mass loss along the marginal area, minus the SMB contribution), which dominates the total ice loss rate of 35.8 ± 10.3 Gt year^{-1}. However, the data also reveal substantial DIL between 1985 and 2002, which in total is larger than the observed DIL from 2005 to 2010. GRACE data show that the ice mass loss in the region was insignificant between 2003 and 2005 (Fig. 1A), which constrains the early loss event to have occurred before 2003. It is likely, though, that most of this occurred over a shorter time period. ATM laser altimetry results from flights in 1994 and 1999 show, even though their coverage is limited, that a substantial part of the surface lowering occurred before those years. For the Gade, Rink, and Kjer glaciers, for example, the ATM data indicate that the entire 1985–2002 elevation difference occurred before 1994 (Table 1 and figs. S1, S9, and S10). Also, data during 1995–2010 from a continuous GPS receiver installed at Thule Airbase suggest huge ice loss during 2005–2010; however, no significant changes occurred during 1995–2005 (Fig. 4). The GPS station was established to determine the vertical crustal motion due to the unloading of ice from nearby glaciers. The GPS data demonstrate constant uplift during 1995–2005, followed by acceleration in July 2005. This indicates that the most recent DIL event started in July 2005, whereas the first event occurred before 1995. Based on the combined ATM and GPS data, we conclude that the entire early ice mass loss occurred over 8 years (1985–1993), and we obtain a rate of 26.6 ± 4.7 Gt year^{-1}, which matches the 25.5 ± 10.4 Gt year^{-1} rate of the most recent ice mass loss event (2005–2010). Thus, the south-north expansion of recent mass loss is not unprecedented, and the DIL could be reoccurring on a multidecadal time scale.

Measurements of mean annual sea surface temperature (SST) from Melville Bugt show positive temperature anomalies that partially coincide with ice loss events in 1985–1994 and more significantly in 2005–2010, suggesting ocean warming as a potential trigger for the widespread glacier acceleration (Fig. 4) (*1*, *21*, *22*). However, the lack of high-resolution SST data, especially in coastal areas where the marine glaciers terminate, prevents a quantitative assessment of the impact of ocean warming. We also find that higher summer air temperatures (recorded at three stations) in northwest Greenland coincided with the most recent mass loss events, implying that part of the ice loss was caused by increased surface melting. The rather modest response in SMB as compared to the observed annual increase in air temperature of +0.20°C year^{-1} in the Melville Bay region of northwest Greenland from 1981 to 2010 reflects the fact that much of the atmospheric warming occurs in the winter, with limited impact on the SMB (*23*). Detailed analysis of the SMB constituents during the past decade has furthermore demonstrated that changes in precipitation patterns from higher to lower accumulation rates around 2005 in northwest Greenland explain much of the interannual variability and the rapid transition to stronger negative mass balances (*24*). During the first event, changes in the SMB did not contribute significantly to the mass loss (Fig. 4A), and ocean warming was probably the main factor to trigger a dynamic ice loss event. However, during the second event, SMB comprised ~33% of the total mass loss in the marginal zone (Table 1), suggesting that the Greenland Ice Sheet is becoming increasingly sensitive to atmospheric warming.

Our results demonstrate that northwestern Greenland, a key area for rapid ice sheet mass changes (*9*), experienced two DIL events in the past three decades. This implies that mass change of the northern Greenland Ice Sheet is not only a result of predictable surface processes over decadal time scales, but is foremost due to 3- to 5-year DIL events that are neither regionally systematic nor monotonic, despite a possible common oceanic forcing. Until this spatial and temporal variability in ice sheet dynamics has been resolved in ice sheet models, we will not be able to realistically predict future sea-level contributions from the Greenland Ice Sheet. Analysis of historical aerial photographs has the potential to explain the patterns of short-lived dynamical ice loss and, in the case of the Greenland and Antarctica Ice Sheets, can extend back to the 1930s and 1940s, when extensive aerial mapping took place. Such analysis may further provide a new observational standard for the temporal and spatial variability of

Table 1. Mass change estimates from the northwest ice margin and northwest drainage basin used in this study. AirDEM1985, aerophotogrammetrical DEM, 1985; ERS, European Remote Sensing satellite; n.a., not applicable.

Period	Volume change (km^3)	Trend/mass (Gt year^{-1})	Ice loss	Method/sensor
		Northwest ice margin		
1985–2005	248 ± 41	–11.4 ± 1.9	Total	AirDEM1985, ATM, ICESat
	17 ± 2	–0.8 ± 0.1	SMB	RACMO2
	231 ± 41	–10.6 ± 1.9	DIL	AirDEM1985, ATM, ICESat, RACMO2
2005–2010	190 ± 56	–35.8 ± 10.3	Total	AirDEM1985, ATM, ICESat
	63 ± 9	–11.6 ± 1.7	SMB	RACMO2
	127 ± 58	–25.5 ± 10.4	DIL	AirDEM1985, ATM, ICESat, RACMO2
		Northwest drainage basin		
1992–2002		3.0 ± n.a.	Total	ERS-1 and -2*
2002–2009		–35.0 ± 4.7	Total	ICESat†
2002–2009		–41.1 ± 8.1	Total	GRACE†
2002–2009		–38.9 ± n.a.	Total	GRACE‡
2003–2007		–33.0 ± n.a.	Total	ICESat§
2002–2007		–29.0 ± 9.0	Total	GRACE‖
2002–2010		–34.5 ± 5.4	Total	GRACE
2005–2010		–46.4 ± 8.9	Total	GRACE

*DS 8 of Zwally *et al*. (*27*). †Region 6 of Ewert *et al*. (*28*). ‡Region 10 and 50% of region 9 of Chen *et al*. (*29*). §DS 8 of Zwally *et al*. (*27*). ‖Region 8 of Wouters *et al*. (*30*). No numbers are from the present study.

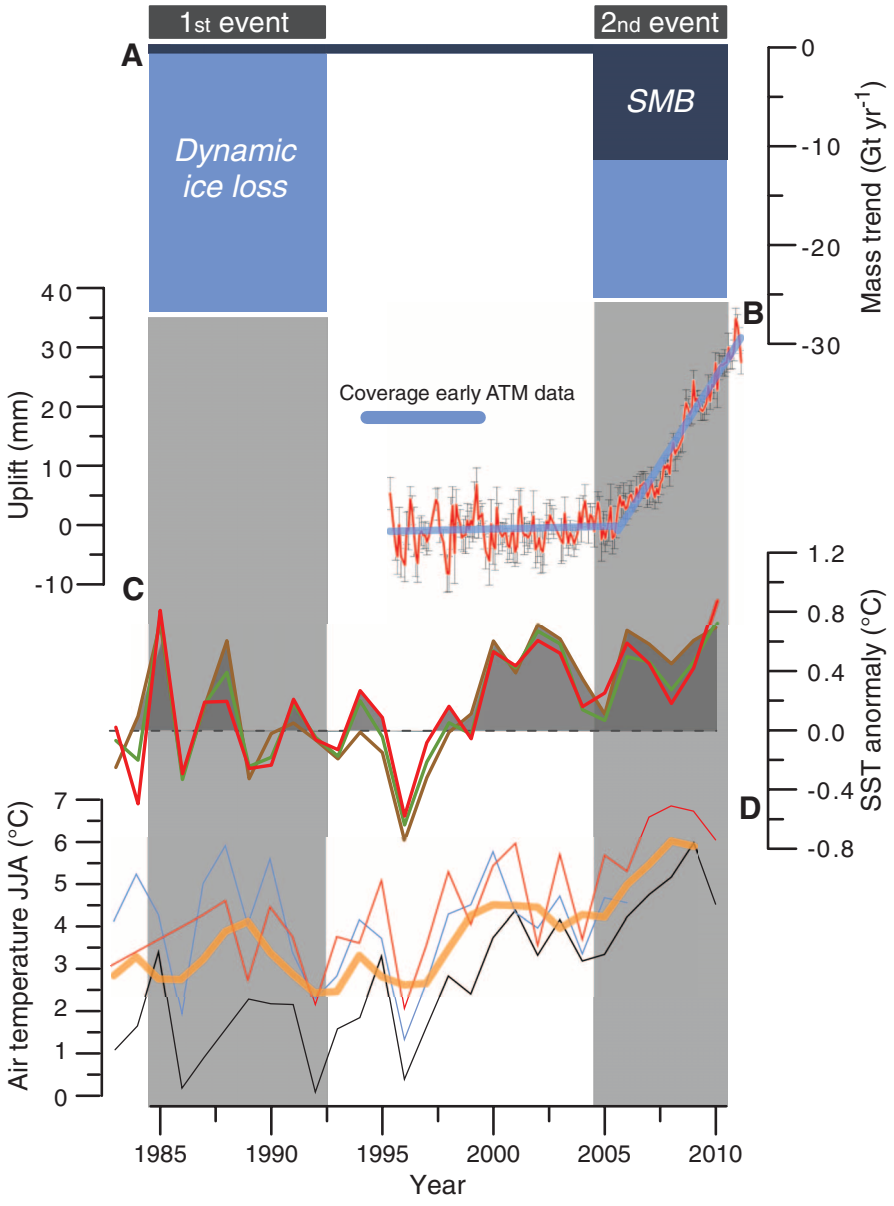

Fig. 4. Ice mass changes and climate records from 1985–2011. (**A**) Mass loss estimate from this study, separated into two distinct events: 1985–1993 and 2005–2010. (**B**) Monthly averages of GPS vertical displacements and their assigned errors at Thule. We fitted a trend to the June 1995–June 2005 data and removed it from the entire time span, to focus on the changes in the trend after 2005 (supplementary materials). The solid lines show the best-fitting linear term to the data during June 1995–June 2005 (which has been set to 0.0 mm year^{-1}) and a trend of 5.9 ± 0.2 mm year^{-1} to data during July 2005–February 2011. (**C**) Mean annual SST anomaly from the International Research Institute for Climate and Society (http://iridl.ldeo.columbia.edu/SOURCES/.NOAA/.NCEP/.EMC/.CMB/.GLOBAL/.Reyn_SmithOIv2/.monthly/.ssta/). The SST is relative to a 1971–2000 baseline. Brown line, ts 1; green line, ts 2; red line, ts 3. For the site location, see Fig. 2C. (**D**) Mean summer [June, July, and August (JJA)] air temperature from Upernavik (red), Kitsissorsuit (black), and Pituffik (blue) meteorological stations (*26*). Orange shows a 3-year running mean.

the ice sheet response that must be met in order to inspire confidence in calculations of the future ice sheet contribution to sea-level rise.

References and Notes

1. D. M. Holland, R. H. Thomas, B. de Young, M. H. Ribergaard, B. Lyberth, *Nat. Geosci.* **1**, 659 (2008).
2. R. H. Thomas *et al.*, *J. Glaciol.* **49**, 231 (2003).
3. I. M. Howat, A. Eddy, *J. Glaciol.* **57**, 389 (2011).
4. F. M. Nick, A. Vieli, I. M. Howat, I. Joughin, *Nat. Geosci.* **2**, 110 (2009).
5. H. D. Pritchard, R. J. Arthern, D. G. Vaughan, L. A. Edwards, *Nature* **461**, 971 (2009).
6. M. R. van den Broeke *et al.*, *Science* **326**, 984 (2009).
7. I. M. Howat, I. Joughin, T. A. Scambos, *Science* **315**, 1559 (2007).
8. S. A. Khan, J. Wahr, M. Bevis, I. Velicogna, E. Kendrick, *Geophys. Res. Lett.* **37**, L06501 (2010).
9. I. Velicogna, *Geophys. Res. Lett.* **36**, L19503 (2009).
10. I. Joughin, B. E. Smith, I. M. Howat, T. Scambos, T. Moon, *J. Glaciol.* **56**, 415 (2010).
11. AMAP, *The Greenland Ice Sheet in a Changing Climate: Snow, Water, Ice and Permafrost in the Arctic (SWIPA) 2009* [Arctic Monitoring and Assessment Programme, (AMAP), Oslo, Norway, 2009].
12. E. Rignot, I. Velicogna, M. R. van den Broeke, A. Monaghan, J. Lenaerts, *Geophys. Res. Lett.* **38**, L05503 (2011).
13. T. Jacob, J. Wahr, W. T. Pfeffer, S. Swenson, *Nature* **482**, 514 (2012).
14. H. J. Zwally *et al.*, GLAS/ICESat L2 Antarctic and Greenland Ice Sheet Altimetry Data V031 (NASA Distributed Active Archive Center at the National Snow and Ice Data Center, Boulder, CO, 2011).
15. W. B. Krabill, IceBridge ATM L2 Icessn Elevation, Slope, and Roughness [1993-2010] (NASA Distributed Active Archive Center at the National Snow and Ice Data Center, Boulder, CO, 2010); http://nsidc.org/data/ilatm2.html.
16. J. Ettema *et al.*, *Geophys. Res. Lett.* **36**, L12501 (2009).
17. J. Ettema *et al.*, *Cryosphere* **4**, 511 (2010).
18. J. Ettema, M. R. van den Broeke, E. van Meijgaard, W. J. van de Berg, *Cryosphere* **4**, 529 (2010).
19. N. Reeh, *J. Geophys. Res.* **113**, F03023 (2008).
20. N. Reeh, D. A. Fisher, R. M. Koerner, H. B. Clausen, *Ann. Glaciol.* **42**, 101 (2005).
21. F. Straneo *et al.*, *Nat. Geosci.* **3**, 182 (2010).
22. T. Murray *et al.*, *J. Geophys. Res.* **115**, F03026 (2010).
23. D. Van As, *J. Glaciol.* **57**, 208 (2011).
24. I. Sasgen *et al.*, *Earth Planet. Sci. Lett.* **333-334**, 293 (2012).
25. J. Wahr, M. Molenaar, F. Bryan, *J. Geophys. Res.* **113**, 30.205 (1998).
26. L. S. Carstensen, B. V. Jørgensen, *Weather and Climate Data from Greenland 1958–2010* (DMI Technical Report Tr 11-10, Danish Meteorological Institute, 2011); www.dmi.dk/dmi/tr11-10.pdf.
27. H. J. Zwally *et al.*, *J. Glaciol.* **57**, 88 (2011).
28. H. Ewert, A. Groh, R. Dietrich, *J. Geodyn.* (2011).
29. J. L. Chen, C. R. Wilson, B. D. Tapley, *J. Geophys. Res.* **116**, B07406 (2011).
30. B. Wouters, D. Chambers, E. J. O. Schrama, *Geophys. Res. Lett.* **35**, L20501 (2008).

Acknowledgments: This work is a part of the RinkProject, within the Centre for GeoGenetics, funded by the Danish Research Council, grant no. 272-08-0415, and the Commission for Scientific Research in Greenland. J.L.B. and R.H. were supported by funding from the ice2sea program from the European Union 7th Framework Programme, grant number 226375. J.W. was partially supported by NASA grants NNX08AF02G and NNXI0AR66G, and by NASA's Making Earth Science Data Records for Use in Research Environments (MEaSUREs) program. M.v.d.B. acknowledges support from Utrecht University and the Netherlands Polar Program. Finally, we extend our gratitude toward the Danish National Cadastre and Survey for facilitating the erection of AirBase: a database containing registrations of aerial photographs from Greenland and their metadata. K.H.K., S.A.K., N.K.L., and E.W. wrote the majority of the main text with significant input from all authors. All authors contributed with interpretation and discussion of results. N.J.K. completed the aerial photogrammetric and validation analyses together with L.H.T., K.H.K., L.T.J., and A.F.-J. J.W. provided the GRACE data and analyses. K.K.K. handled the Geographical Information System and database management. J.B., M.v.d.B., and R.H. provided SMB and firn density data. A.A.B., L.H.T., and N.K.L. collected ice marginal data and analyzed their long-term significance.

Supplementary Materials

www.sciencemag.org/cgi/content/full/337/6094/569/DC1
Materials and Methods
Figs. S1 to S10
References

15 February 2012; accepted 22 June 2012
10.1126/science.1220614